Research Article | Vol. 27, No. 24 / 25 November 2019 / Optics Express 35267
Optics EXPRESS

Piezo-enhanced acoustic detection module for mid-infrared trace gas sensing using a grooved quartz tuning fork

SHANGZHI LI,[1,2] HONGPENG WU,[1,2] RUYUE CUI,[1,2] ANGELO SAMPAOLO,[3] PIETRO PATIMISCO,[3] VINCENZO SPAGNOLO,[1,3,5] FRANK K. TITTEL,[4] AND LEI DONG[1,2,*]

[1] *State Key Laboratory of Quantum Optics and Quantum Optics Devices, Institute of Laser Spectroscopy, Shanxi University, Taiyuan 030006, China*
[2] *Collaborative Innovation Center of Extreme Optics, Shanxi University, Taiyuan 030006, China*
[3] *PolySense Lab – Dipartimento Interateneo di Fisica, University and Politecnico of Bari, Via Amendola 173, Bari, Italy*
[4] *Department of Electrical and Computer Engineering, Rice University, Houston, Texas 77005, USA*
[5] *vincenzoluigi.spagnolo@poliba.it*
[*] *donglei@sxu.edu.cn*

Abstract: A grooved quartz tuning fork (QTF) with a prong spacing of 800 μm for QEPAS application is reported. The prongs spacing is large enough to facilitate optical alignments when a degraded laser beam is used for QEPAS-based trace gas sensors. The grooved QTF has a resonance frequency of 15.2 kHz at atmospheric pressure and is characterized by four rectangular grooves carved on the QTF prong surfaces. With a grooved-prong, the electrical resistance R of the QTF is reduced resulting in an enhanced piezoelectric signal, while the Q factor is not affected, remaining as high as 15000 at atmospheric pressure. The geometric parameters of the acoustic micro resonators (AmRs) for on-beam QEPAS were optimized to match the grooved QTF, and a signal-to-noise gain factor of ~ 30 was obtained with an optimum configuration. The performance of the QEPAS-based sensor was demonstrated exploiting an interband cascade laser (ICL) for CH_4 detection and a 1σ normalized noise equivalent absorption (NNEA) coefficient of 4.1×10^{-9} cm^{-1} W/$\sqrt{\text{Hz}}$ was obtained at atmospheric pressure.

1. Introduction

Trace gas sensing techniques have an important impact on different application fields, such as environmental monitoring, combustion processes, agricultural biogas detection and medical diagnostics [1–7]. Quartz enhanced photoacoustic spectroscopy (QEPAS), which employs a quartz tuning fork (QTF) as resonant acoustic transducer, is one of the most sensitive and selective trace gas detection techniques [8–10]. In QEPAS based sensors, QTF is a crucial part which converts resonant vibration induced by the interaction of gas molecule and modulated optical radiation into electric signal by means of the piezoelectric effect. Due to the high resonance frequency (f_0) and high quality factor (Q), QEPAS system is immune to ambient acoustic noise. In addition, with the advantages of simple structure and small size, only a few tens cubic millimeters of target gas are needed, so that QTF based QEPAS gas sensors are more compact and reliable in certain applications [11–22].

In QEPAS, to retrieve the photoacoustic signal the sound source must be located between the QTF prongs, implying that the laser beam must be focused on the QTF plane and through the gap between the prongs [23]. Most QEPAS sensors reported in the literature exploit a standard QTF characterized by a fundamental in-plane flexural mode with f_0 ~ 32.768 kHz. Nevertheless, due to the narrow prong spacing (300 μm) of the 32 kHz QTF, an undesirable nonzero background

#372892 https://doi.org/10.1364/OE.27.035267
Journal © 2019 Received 16 Jul 2019; revised 31 Oct 2019; accepted 11 Nov 2019; published 18 Nov 2019

Optics EXPRESS

noise (photo-thermal noise) will arise when a portion of the laser light beam hits the QTF. This can occur when employing a laser source with a degraded beam profile such as interband cascade lasers (ICLs), quantum cascade lasers (QCLs) and THz lasers. When spatial beam filters are used, the footprint of the sensing system significantly increase [24–26]. Recently, custom-made QTFs with larger prongs spacing (600-800 μm) were realized and implemented in QEPAS gas sensors, allowing the operation with fiber amplified and THz QCL light sources [27–29]. These custom-made QTFs were designed to operate at lower resonance frequency down to a few kHz to satisfy the condition $f_0 \ll \frac{1}{2\pi\tau}$ (τ is the molecular relaxation time) also for gas species characterized by slow vibrational-translational relaxation rate, such as NO, CO, CO_2 and CH_4 [30,31]. As reported in [32], the QTF quality factor Q is negatively affected by decreasing the resonance frequency f_0, leading to an attenuation of detected signal and deterioration of sensor performance. The biggest challenge in the design of QTFs is to reduce the f_0 while keeping high the Q factor. Hence, several prong geometries were designed, realized and tested by measuring the QTF resonance performance. Novel variants of the QTF geometry were also proposed. The prong spacing of the QTF was increased up to 1.5 mm, grooves were carved on the QTF prongs [33] and T-shaped prong geometries were also investigated [34]. All these new geometries were realized by standard photolithographic technique and chemical etching [35].

To further improve the performance of QEPAS sensors, acoustic micro resonators (AmRs), which consist of single or pair of stainless-steel tubes are employed to confine and amplify sound waves [36]. The QTF acoustically coupled with the AmRs is often identified as a QEPAS spectrophone, which is the key component of the acoustic detection module (ADM) which also includes a gas cell, optical windows and gas-in and -out connectors. AmRs can improve the signal-to-noise (SNR) gain factor, defined as the ratio between the SNR of QTFs with and without the AmRs, by more than one order of magnitude. To date, two main ADM configurations, on-beam and off-beam, have been proposed for QEPAS sensing [9,37], but the on-beam configuration offers a higher SNR gain factor. The optimal geometrical parameters of the AmRs, such as tubes length, inner tubes diameter and their positions strictly depend on the QTF geometry and its resonance properties.

In this work, we report on a custom QTF exploiting rectangular grooves on both surfaces of the QTF prongs, characterized by a $f_0 \sim 15.2$ kHz, with Q factor ~ 15000. The presence of four rectangular grooves results in a reduced $R \sim 110$ kΩ at atmospheric pressure and thus enhances the piezoelectric effect of the QTF. The prong spacing of the QTF is 800 μm, allowing to employ laser sources such as an ICL or QCL to be focused through the prong spacing without being blocked by the QTF itself. QEPAS measurements were performed to optimize the geometrical parameters of the AmRs for the grooved QTF employing C_2H_2:N_2 as test gas mixture. We investigate the performance of the optimized grooved QTF ADM to trace methane (CH_4) in air employing an ICL as excitation source.

2. Experiment

2.1. Grooved QTF

The electrical parameters of QTFs depend strongly on their geometries [38]. To design a QTF for QEPAS applications, the main guidelines are the following: (1) the prong spacing should be large enough to simplify the optical alignment and minimize the photo-thermal noise; (2) the fundamental resonance frequency f_0 of the QTFs should be reduced to improve the QEPAS response especially when dealing with gas species characterized by slow non-radiative relaxation rates; (3) the Q-factor should be as high as possible since the QEPAS signal is proportional to the QTF Q-factor. Modeling of the QTF prong as a single cantilever, the fundamental resonance

Optics EXPRESS

frequency can be determined by using the Euler-Bernoulli equation:

$$f_0 = \frac{1.194^2 \pi W}{8\sqrt{12}L^2}\sqrt{\frac{E}{\rho}} \tag{1}$$

where W, L, E and ρ are the prong width, prong length, quartz Young modulus (0.72×10^{11} N/m^2) and density (2.65×10^3 kg/m^3), respectively [37]. For this work, a QTF frequency operation of ~ 15 kHz was selected. The Q-factor of a QTF is related to the loss mechanisms occurring while the QTF is vibrating and represents the ratio of energy stored to energy dissipated per cycle. The main contributions are due to the interaction with the surrounding medium, damping of the prong base and thermoelastic losses. According to the experimental investigation [32,38], the Q-factor can be phenomenologically related to the prong geometry by the relation:

$$Q = 3.78\times10^5 \frac{WT}{L} \tag{2}$$

where T is the thickness of the QTF and all the units are in millimeters. Then, f_0 and the Q-factor are clearly correlated. To ensure the QTF can be driven effectively by the sound waves, the prong width W must be less than 10-times thickness T. Using Eqs. (1) and (2), the geometrical parameters providing the highest Q-factor (~16000) at $f_0 = 15$ kHz are $L = 9.4$ mm and $W = 2$ mm, while T is fixed at 0.25 mm. Starting from this QTF geometry, a 800 μm prong spacing was selected. The electrical resistance R is also a crucial parameter of a QTF which determines the piezoelectric current value when a voltage excitation is applied across the QTF at the resonance frequency. A QTF can be modelled as an RLC series circuit $Q = 1/(2\pi f_0 RC)$ where C *is* the QTF capacitance, i.e. the coupling between the electrodes and the resonance mode. Thereby, if the Q-factor and f_0 can be considered as a constant, by maintaining fixed the prong length and thickness, an increase of C will provide a reduction of R, thus improving the piezoelectric current and enhancing piezoelectric effect. An increase of C (without varying L and W) can be obtained by reducing the distance between positive and negative QTF electrodes. This can be done by carving grooves on the prongs surfaces. As depicted in Fig. 1, rectangular grooves 0.05 mm depth with an area of 1.8×7 mm^2 were carved on each QTF prong surface. The central electrodes were deposited on the grooved surface. Such surface modification provide a 30% reduction of the R value without affecting the Q-factor as predicted.

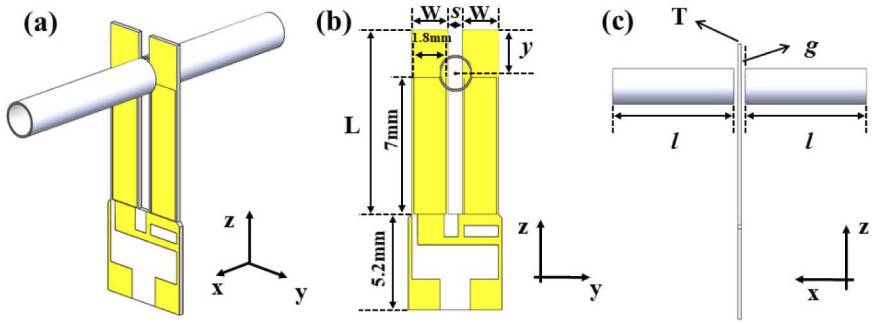

Fig. 1. (a) Schematic of on-beam spectrophone based on a grooved QTF, The tubes were centered between the QTF prongs; (b), (c) geometric parameters of the on-beam spectrophone, where L is the prong length, W is the width, T is the thickness, s is the prong spacing, y is the distance from QTF top surface to the tube center, l is the AmR length, and g is the QTF-tube distance.

Optics EXPRESS

2.2. On-beam spectrophone configuration

The on-beam spectrophone consists of a grooved QTF with a resonance frequency of 15.2 kHz acoustically coupled with a pair of stainless-steel tubes (see Fig. 1). The two tubes are symmetrically positioned on both sides of the QTF and aligned perpendicular to the QTF plane, confining the sound wave and amplifying the QEPAS signal. If we assume the distance g between the QTF and tubes as zero, the two tubes can be considered in a first approximation as a single half-wavelength resonator with a length ($2\,l$) of $\lambda_a/2$, where λ_a is the acoustic wavelength. However, the insertion of the QTF between the two tubes causes a distortion of the acoustic resonance in the resonator, resulting in an optimal full length of the resonator between $\lambda_a/2$ and λ_a. Therefore, to improve the QEPAS signal, the optimum length l of each tube is $\lambda_a/4 < l < \lambda_a/2$ [36,39].

Beside the tubes length l, the other parameter governing the spectrophone performance is the inner diameter (ID) of the tubes, which is strictly related with the prong spacing and determines the overall volume of the excited gas. When the tube diameter is larger than the prongs spacing, the effect of the gap between two tubes becomes negligible and the tubes are well acoustically coupled with the QTF. However, if the tubes diameter becomes much larger than the prongs spacing the acoustic coupling with the QTF decreases, weakening the amplification effects of the AmRs. When employing AmRs with ID comparable or smaller than the prongs spacing, the optical energy absorbed by gas molecules decreases due to the reduced gas volume inside the tubes, leading to a QEPAS signal decreasing. Hence, we tested different geometric parameters of the AmRs to retrieve the optimal configuration. The results of this study are described in the following section.

2.3. Experimental setup

The experimental setup is schematically depicted in Fig. 2. A fiber-coupled distributed feedback (DFB) diode laser (NTT Electronics Corporation model NLK1C5J1AA) with a 14-pin butterfly package emitting at 1.53 μm is used as the QEPAS excitation light source in order to optimize the ADM parameters . A custom-made control electronics unit (CEU) was employed to control the DFB laser temperature and current. The CEU was also capable to determine the electrical parameters (f_0, Q, R) of QTF and to lock the laser emission wavelength to the target gas selected absorption line. The laser beam was collimated by a fiber-coupled collimator (OZ optics Ltd. Model LPC-01) with a spot diameter of 200 μm, so that it could easily pass through the ADM. Two 25.4-mm diameter CaF_2 windows with 97% transmissivity efficiency were mounted on the gas cell for optical access. The gas cell has an inner volume of 70 cm^3. A power meter (Ophir Optronics Solutions. LTD, Israel, Model 3AROHS) was placed after the ADM for alignment purpose and to monitor the transmitted laser power. A pressure controller (MKS Instrument Inc., U.S.A., Model 649B) was utilized to control the pressure inside the gas cell, in combination with a mini diaphragm pump (KNF Technology Co., Ltd., Germany, Model N813.5ANE). A flow meter (Alicat Scientific, Inc. Model M-500SCCMD) was used to monitor the gas flow rate, which can be adjusted using needle valve. The flow rate was maintained at a constant value of 60 sccm in all measurements to obtain a low flow noise, which results in a gas exchange time of 75 s.

The 2f-wavelength modulation spectroscopy (WMS) detection technique was used for QEPAS detection. The laser central wavelength was tuned by applying a slow voltage ramp to the laser and a high frequency sinusoidal component at half of the grooved QTF resonance frequency ($f_0/2$ ~ 7.6 kHz). The piezoelectric signal generated by the QTF was amplified by a trans-impedance pre-amplifier (PA) with a 10-MΩ feedback resistor (R_g) and sent to the lock-in amplifier (Stanford Research Systems, Model SR830), which demodulated the photoacoustic signal into a second harmonic signal with a filter slope of 12 dB/oct and a time constant of 300 ms, leading to a 0.833 Hz detection bandwidth.

Optics EXPRESS

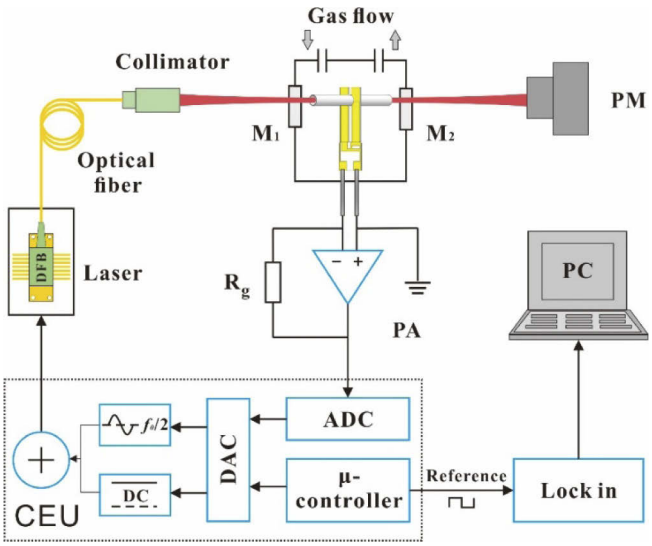

Fig. 2. Schematic diagram of the QEPAS-based sensor system. M_1, M_2: CaF_2 windows; PM: power meter; PA: pre-amplifier and CEU: control electronics unit.

3. Results and discussion

3.1. On-beam ADM optimization

In order to determine the performance of the grooved-QTF based-QEPAS sensor, acetylene (C_2H_2) was selected as the target gas. The C_2H_2 is characterized by a fast Vibration-Translation (V-T) relaxation time of ~ 0.1 μs [40]. According to the HITRAN database, a C_2H_2 absorption line at 6529.17 cm^{-1} with a line intensity of 1.16×10^{-20} cm/mol was chosen and a 30 ppm C_2H_2:N_2 mixture was used as target gas mixture.

To optimize the on-beam ADM geometry, the optimal vertical position where positioning the two tubes must be determined. The laser beam was focused along the QTF symmetry axis and a vertical scan was performed while retrieving the QEPAS intensity. The signal obtained by tuning the vertical distance y between the QTF top surface and the laser focus from 0 to 9 mm is shown in Fig. 3. The data are normalized to the maximum value and the optimum laser focus position of y was determined to be 1.5 mm far from the prong top. Once determining the optimal vertical position for the micro resonator tubes an optimization of their geometry was carried out.

Figure 4 shows the comparison between the QEPAS SNRs measured employing AmRs with different lengths and IDs in the pressure range from 25 Torr to 700 Torr. According to the previous assumptions and considering the sound wavelength of $\lambda_a = 22.4$ mm at 15 kHz, the length l of each tube was varied in the range 7 mm < l < 12 mm, while four different IDs, ID = 1.3 mm, 1.5 mm, 1.65 mm, 1.85 mm were selected. The distance between the grooved QTF and tubes was set at 100 μm. For all AmRs, starting from 700 Torr to lower pressures, the QEPAS SNR increased gradually until a maximum was reached which differs from AmR to AmR. Then the SNR rapidly decreases towards lower pressures. The pressure providing the peak SNR value depends upon the tubes lengths. The overall maximum SNR of 338 was achieved at a pressure of 200 Torr when the tube dimensions were ID = 1.65 mm and l = 9 mm.

In Fig. 5, the QEPAS SNRs measured for tubes 9 mm long with different IDs are compared. At atmospheric pressure, the SNR value (~ 200) achieved with 1.85-mm ID tubes is similar to that measured for 1.65-mm-ID tubes and 17% higher than that measured with the other two IDs. For comparison, the SNR tested with a bare grooved QTF without AmRs is also shown.

Optics EXPRESS

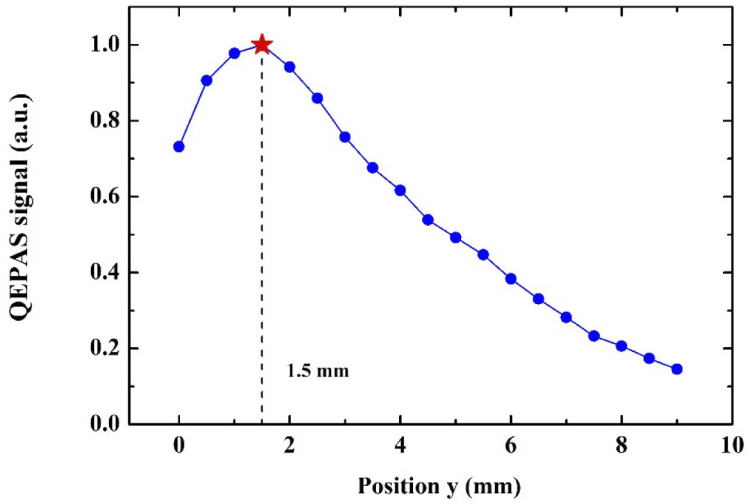

Fig. 3. The normalized QEPAS signal amplitude as a function of the position *y* along the vertical axis of the QTF.

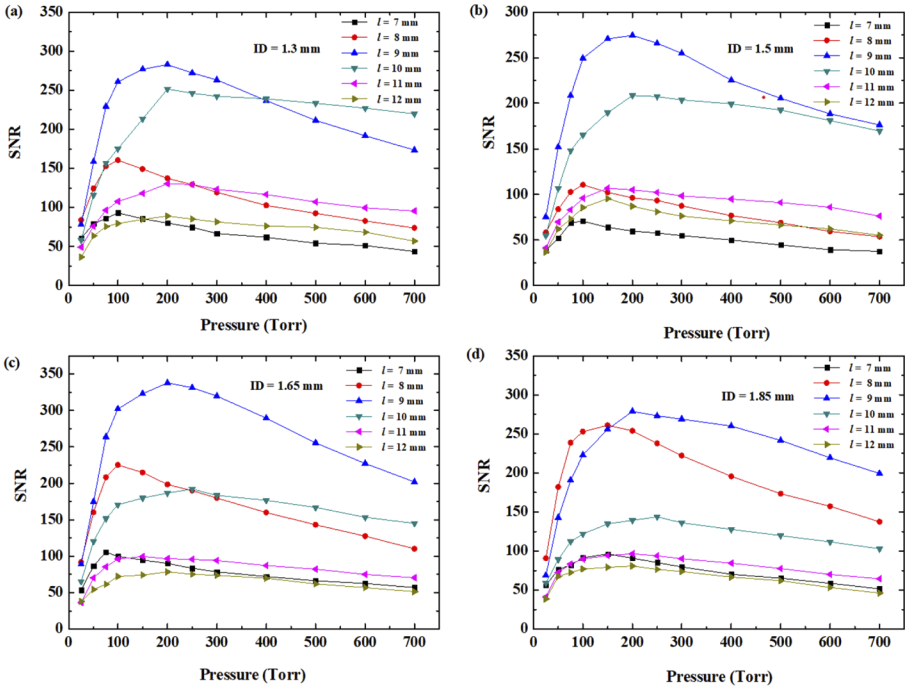

Fig. 4. The SNR as a function of the pressure inside the ADM with different acoustic resonators. Data are obtained by detecting a concentration of 30-ppm C_2H_2 in N_2 from 25 Torr to 700 Torr. *l*: tube length; ID: inner diameter of the tube.

Optics EXPRESS

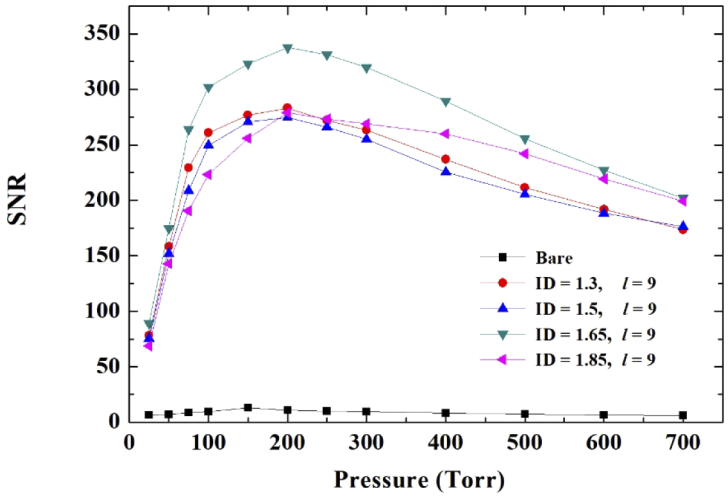

Fig. 5. The SNR as a function of gas pressure for bare QTF and spectrophones employing AmRs with an ID = 1.3 mm, 1.5 mm, 1.65 mm, 1.85 mm but the same length.

After selecting the best geometry for the tubes (ID = 1.65 mm, l = 9 mm), the dependence of the distance g between the QTF and tubes, which is also a key parameter related to the ADM performance was investigated in the range of 20 μm < g < 1200 μm. The measured SNRs are shown in Fig. 6 as a function of g at atmospheric pressure. The SNR is improved by only 2% when the g increased from 20 to 150 μm, confirming that an excellent acoustic coupling is achieved in such a range. This condition is no more valid when g becomes larger than 200 and at 1200 μm approached the value measured for the bare QTF. Hence, the optimal geometric parameters of the AmRs were determined to be l = 9 mm, ID = 1.65 mm and g = 100 μm.

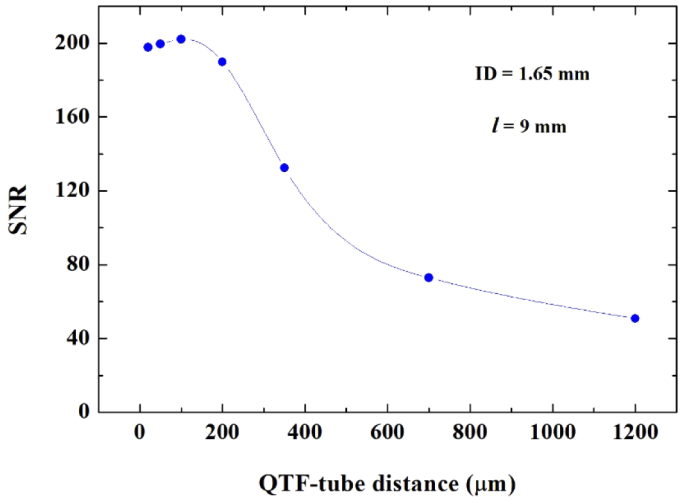

Fig. 6. The SNR as a function of the distance between the tubes and the grooved QTF measured from 20 μm to 1200 μm.

Figure 7 shows the 2f-spectrum measured for the bare QTF and the QTF plus AmR for a 30-ppm C_2H_2:N_2 mixture at 700 Torr. The laser current was scanned from 167 mA to 207 mA operating at 35.5 °C and the optical power at the C_2H_2 absorption peak was 22.7 mW. The SNR

Optics EXPRESS

measured with the optimum AmR configuration is ~ 319, corresponding to a gain factor of ~ 30 with respect to the bare QTF and resulting in a 1σ minimum detection limit (MDL) of 94 ppb. The corresponding normalized noise equivalent absorption (NNEA) coefficient is 2.73×10^{-9} $cm^{-1}W/\sqrt{Hz}$.

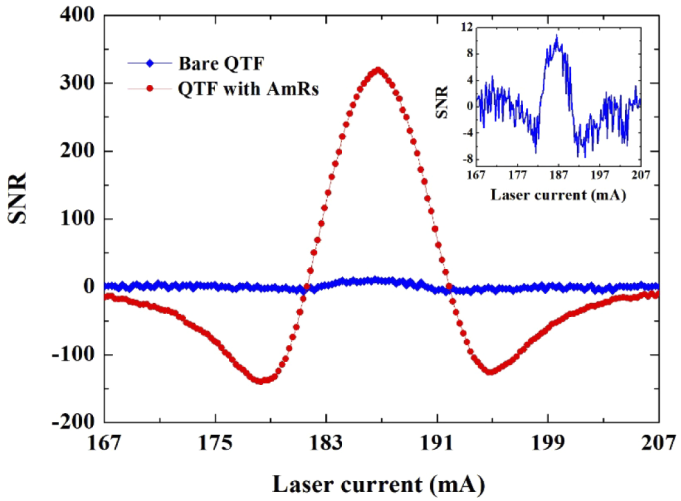

Fig. 7. The second-harmonic QEPAS spectra of C_2H_2 absorption line with the optimum AmRs (l = 9 mm, ID = 1.65 mm) and bare grooved QTF at atmospheric pressure (700 Torr). In the inset, an amplified view of the bare QTF signal is shown.

3.2. CH_4 detection for performance assessment

The next step was an investigation of the mid-infrared performance of the reported QEPAS ADM with optimum AmRs for CH_4 detection. For this purpose, an interband cascade laser (ICL) (Nanoplus model 2199/1-6) was employed. The temperature and current of the ICL were controlled by a temperature controller (Thorlabs, Model TED200C) and a current driver (Wavelength Electronics, Model QCL2000LAB). At 10°C of laser temperature, the ICL targets a CH_4 absorption line located at 3038.5 cm^{-1} with a line strength of 8.678×10^{-20} cm/mol, with an optical power of 1.8 mW. A plano-convex CaF_2 lens with a focal length of 75 mm was used to focus the laser beam. The laser spot size at the focal point has a diameter of ~400 μm, which is half of the QTF prong spacing.

A certified 30-ppm CH_4:N_2 gas mixture (Nanjing Special Gas Factory Co., Ltd.) was flushed into the ADM with a flow rate of 60 sccm near atmospheric pressure using a Nafion tube to fix the water concentration at 1.7%. In this way, any promoter relaxation effect from H_2O vapor is kept constant. CH_4 samples with concentration spanning from 2 ppm to 30 ppm were realized by using a gas dilution system (Environics Inc. Model EN4000), starting from the certified mixture. The QEPAS signals at CH_4 different concentrations were acquired and peaks values are shown in Fig. 8. Each peak value was measured multiple times and averaged. A linear fitting with R square value of 0.9992 confirms the linear response of the sensor system in the investigated CH_4 concentration range. The noise level is 1.16 μV and the MDL achieved was 210 ppb, corresponding to a NNEA coefficient of 4.1×10^{-9} $cm^{-1}W/\sqrt{Hz}$.

In order to analyze the long-term stability of the CH_4 QEPAS sensor, an Allan-Werle variance analysis with 2f-WMS technique was performed as a function of the averaging time. Pure N_2 was flushed into the sensor and the laser wavelength was locked at the CH_4 absorption line peak. From the Allan deviation plot shown in Fig. 9, the sensitivity can be improved by further

Optics EXPRESS

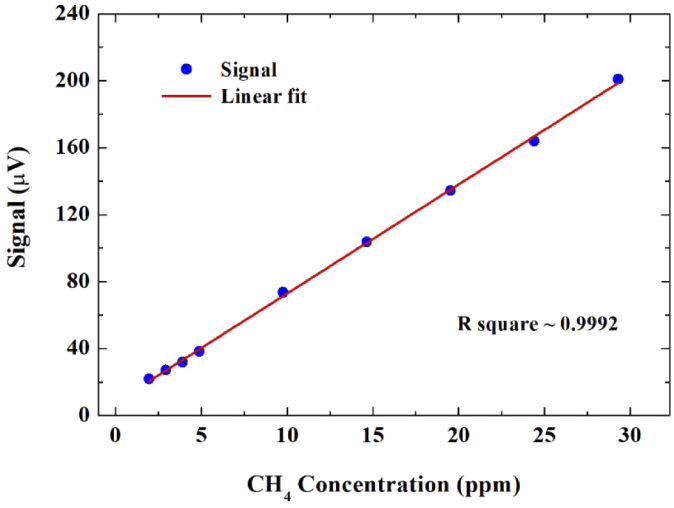

Fig. 8. The QEPAS signals at different CH_4 concentration levels. The red line represents the linearity of the sensor system response.

increasing the averaging time and an optimum averaging time of 400 s resulted in a MDL of ~15 ppb.

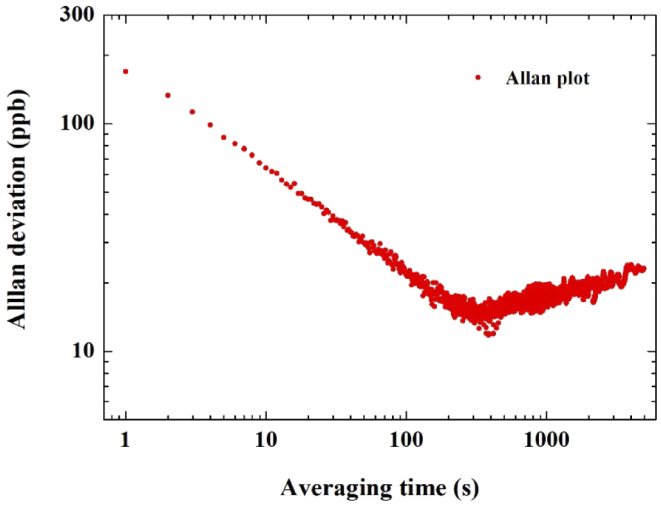

Fig. 9. Allan-Werle deviation plot for different averaging time measured with pure N_2 for the QEPAS based sensor system.

To detect atmospheric CH_4 concentrations, the ambient air outside the laboratory was pumped into the QEPAS sensor using a Nafion tube to fix the water concentration at 1.7%. The measurement was carried out with a 1-s acquisition time near atmospheric pressure and the obtained results are shown in Fig. 10. The laser current was scanned from 20 mA to 42 mA for a whole 2*f* QEPAS signal of CH_4 absorption line. The detected QEPAS peak signal was 25.6 μV, and the ambient CH_4 concentration was calculated to be 2.3 ppm.

Optics EXPRESS

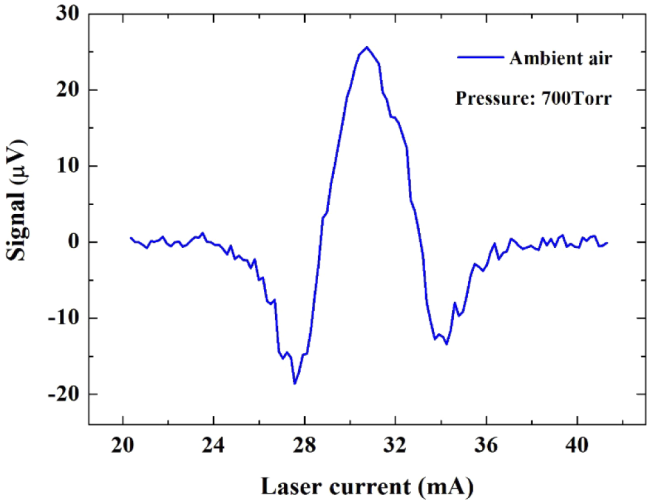

Fig. 10. Experimental measured 2*f*-QEPAS spectra near ambient CH_4 gas at atmospheric pressure.

4. Conclusions

A grooved QTF with a prong spacing of 800 μm was designed and its performance was evaluated. A rectangular groove was carved on each prong surface of the QTF in order to reduce the electrical resistance *R* and to enhance the piezoelectric effect without affecting the *Q*-factor and the resonance frequency f_0. A f_0 of 15.2 kHz was measured, resulting in less than 50% of the standard 32.7-kHz QTF. However, the quality factor of 15,000 was 50% higher than that of a standard QTF at atmospheric pressure in air (typically ~10,000). The geometric parameters of the AmRs for on-beam QEPAS configuration were optimized employing a 30-ppm C_2H_2:N_2 mixture as a test gas mixture. The optimal geometric parameters of the micro resonator tubes composing the AmRs are $l = 9$ mm, ID = 1.65 mm and $g = 100$ μm, providing a SNR gain factor of ~ 30 with respect to the bare grooved QTF. The QEPAS sensor was tested for CH_4 detection exploiting an ICL source. An MDL and NNEA of 210 ppb and 4.1×10^{-9} $cm^{-1}W/\sqrt{Hz}$ at 1 s integration time were achieved, respectively. The sensor was validated for out-of-laboratory air detection, demonstrating its capability to detect atmospheric trace CH_4 concentrations using a mid-infrared laser source.

Funding

National Key R&D Program of China (2017YFA0304203); National Natural Science Foundation of China (11434007, 61575113, 61622503, 61805132); Changjiang Scholars and Innovative Research Team in University of Ministry of Education of China (IRT_17R70); 111 project (D18001); Shanxi "1331KSC" (1331KSC); Robert Welch Foundation (C0586); Foundation for Selected Young Scientists Studying Abroad; Sanjin Scholar (2017QNSJXZ- 04). The authors from Dipartimento Interateneo di Fisica di Bari acknowledge the financial support from THORLABS GmbH within the joint-research laboratory PolySense.

References

1. A. A. Kosterev, G. Wysocki, Y. Bakhirkin, S. So, R. Lewicki, M. Fraser, F. K. Tittel, and R. F. Curl, "Application of quantum cascade lasers to trace gas analysis," Appl. Phys. B: Lasers Opt. **90**(2), 165–176 (2008).
2. G. Wysocki, Y. A. Bakhirkin, S. So, F. K. Tittel, C. J. Hill, R. Q. Yang, and M. P. Fraser, "Dual interband cascade laser based trace-gas sensor for environmental monitoring," Appl. Opt. **46**(33), 8202–8210 (2007).

Optics EXPRESS

3. R. F. Curl, F. Capasso, C. Gmachl, A. A. Kosterev, B. McManus, R. Lewicki, M. Pusharsky, G. Wysocki, and F. K. Tittel, "Quantum cascade lasers in chemical physics," Chem. Phys. Lett. **487**(1-3), 1–18 (2010).
4. L. Dong, W. Yin, W. Ma, L. Zhang, and S. Jia, "High-sensitivity, large dynamic range, auto-calibration methane optical sensor using a short confocal Fabry–Perot cavity," Sens. Actuators, B **127**(2), 350–357 (2007).
5. Z. Li, L. Zhao, W. Tan, W. Ma, G. Zhao, X. Fu, L. Dong, L. Zhang, W. Yin, and S. Jia, "Investigation and cancellation of residual amplitude modulation in fiber electro-optic modulator based frequency modulation gas sensing technique," Sens. Actuators, B **196**, 23–30 (2014).
6. J. Hodgkinson and R. P. Tatam, "Optical gas sensing: a review," Meas. Sci. Technol. **24**(1), 012004 (2013).
7. P. Daukantas, "Air-quality monitoring in the mid-infrared," Opt. Photonics News **26**(11), 26–33 (2015).
8. A. A. Kosterev, Y. Bakhirkin, R. F. Curl, and F. K. Tittel, "Quartz-enhanced photoacoustic spectroscopy," Opt. Lett. **27**(21), 1902–1904 (2002).
9. A. A. Kosterev, F. K. Tittel, D. V. Serebryakov, A. L. Malinovsky, and I. V. Morozov, "Applications of quartz tuning forks in spectroscopic gas sensing," Rev. Sci. Instrum. **76**(4), 043105 (2005).
10. P. Patimisco, A. Sampaolo, L. Dong, F. K. Tittel, and V. Spagnolo, "Recent advances in quartz enhanced photoacoustic sensing," Appl. Phys. Rev. **5**(1), 011106 (2018).
11. M. Mordmüller, M. Köhring, W. Schade, and U. Willer, "An electrically and optically cooperated QEPAS device for highly integrated gas sensors," Appl. Phys. B: Lasers Opt. **119**(1), 111–118 (2015).
12. L. Dong, H. Wu, H. Zheng, Y. Liu, X. Liu, W. Jiang, L. Zhang, W. Ma, W. Ren, W. Yin, S. Jia, and F. K. Tittel, "Double acoustic microresonator quartz-enhanced photoacoustic spectroscopy," Opt. Lett. **39**(8), 2479–2482 (2014).
13. H. Yi, R. Maamary, X. Gao, M. W. Sigrist, E. Fertein, and W. Chen, "Short-lived species detection of nitrous acid by external-cavity quantum cascade laser based quartz-enhanced photoacoustic absorption spectroscopy," Appl. Phys. Lett. **106**(10), 101109 (2015).
14. W. Ren, W. Jiang, N. P. Sanchez, P. Patimisco, V. Spagnolo, C. Zah, F. Xie, L. C. Hughes, R. J. Griffin, and F. K. Tittel, "Hydrogen peroxide detection with quartz-enhanced photoacoustic spectroscopy using a distributed-feedback quantum cascade laser," Appl. Phys. Lett. **104**(4), 041117 (2014).
15. Y. Ma, Y. Tong, Y. He, X. Jin, and F. K. Tittel, "Compact and sensitive mid-infrared all-fiber quartz-enhanced photoacoustic spectroscopy sensor for carbon monoxide detection," Opt. Express **27**(6), 9302–9312 (2019).
16. L. Hu, C. Zheng, J. Zheng, Y. Wang, and F. K. Tittel, "Quartz tuning fork embedded off-beam quartz-enhanced photoacoustic spectroscopy," Opt. Lett. **44**(10), 2562–2565 (2019).
17. S. Borri, P. Patimisco, I. Galli, D. Mazzotti, G. Giusfredi, N. Akikusa, M. Yamanishi, G. Scamarcio, P. De Natale, and V. Spagnolo, "Intracavity quartz-enhanced photoacoustic sensor," Appl. Phys. Lett. **104**(9), 091114 (2014).
18. A. Sampaolo, P. Patimisco, M. Giglio, L. Chieco, G. Scamarcio, F. K. Tittel, and V. Spagnolo, "Highly sensitive gas leak detector based on a quartz-enhanced photoacoustic SF_6 sensor," Opt. Express **24**(14), 15872–15881 (2016).
19. H. Zheng, L. Dong, X. Yin, X. Liu, H. Wu, L. Zhang, W. Ma, W. Yin, and S. Jia, "Ppb-level QEPAS NO_2 sensor by use of electrical modulation cancellation method with a high power blue LED," Sens. Actuators, B **208**, 173–179 (2015).
20. H. Wu, L. Dong, H. Zheng, Y. Yu, W. Ma, L. Zhang, W. Yin, L. Xiao, S. Jia, and F. K. Tittel, "Beat frequency quartz-enhanced photoacoustic spectroscopy for fast and calibration-free continuous trace-gas monitoring," Nat. Commun. **8**(1), 15331 (2017).
21. H. Wu, L. Dong, W. Ren, W. Yin, W. Ma, L. Zhang, S. Jia, and F. K. Tittel, "Position effects of acoustic micro-resonator in quartz enhanced photoacoustic spectroscopy," Sens. Actuators, B **206**, 364–370 (2015).
22. H. Zheng, L. Dong, Y. Ma, H. Wu, X. Liu, X. Yin, L. Zhang, W. Ma, W. Yin, L. Xiao, and S. Jia, "Scattered light modulation cancellation method for sub-ppb-level NO_2 detection in a LD-excited QEPAS system," Opt. Express **24**(10), A752–A761 (2016).
23. F. K. Tittel, A. Sampaolo, P. Patimisco, L. Dong, A. Geras, T. Starecki, and V. Spagnolo, "Analysis of overtone flexural modes operation in quartz-enhanced photoacoustic spectroscopy," Opt. Express **24**(6), A682–A692 (2016).
24. L. Dong, V. Spagnolo, R. Lewicki, and F. K. Tittel, "Ppb-level detection of nitric oxide using an external cavity quantum cascade laser based QEPAS sensor," Opt. Express **19**(24), 24037–24045 (2011).
25. V. Spagnolo, P. Patimisco, S. Borri, G. Scamarcio, B. E. Bernacki, and J. Kriesel, "Mid-infrared fiber-coupled QCL-QEPAS sensor," Appl. Phys. B: Lasers Opt. **112**(1), 25–33 (2013).
26. Y. Ma, R. Lewicki, M. Razeghi, and F. K. Tittel, "QEPAS based ppb-level detection of CO and N_2O using a high power CW DFB-QCL," Opt. Express **21**(1), 1008–1019 (2013).
27. V. Spagnolo, P. Patimisco, R. Pennetta, A. Sampaolo, G. Scamarcio, M. S. Vitiello, and F. K. Tittel, "THz Quartz-enhanced photoacoustic sensor for H_2S trace gas detection," Opt. Express **23**(6), 7574–7582 (2015).
28. A. Sampaolo, P. Patimisco, M. Giglio, M. Vitiello, H. Beere, D. Ritchie, G. Scamarcio, F. K. Tittel, and V. Spagnolo, "Improved Tuning Fork for Terahertz Quartz-Enhanced Photoacoustic Spectroscopy," Sensors **16**(4), 439 (2016).
29. S. Borri, P. Patimisco, A. Sampaolo, H. E. Beere, D. A. Ritchie, M. S. Vitiello, G. Scamarcio, and V. Spagnolo, "Terahertz quartz enhanced photo-acoustic sensor," Appl. Phys. Lett. **103**(2), 021105 (2013).
30. A. Sampaolo, P. Patimisco, L. Dong, A. Geras, G. Scamarcio, T. Starecki, F. K. Tittel, and V. Spagnolo, "Quartz-enhanced photoacoustic spectroscopy exploiting tuning fork overtone modes," Appl. Phys. Lett. **107**(23), 231102 (2015).

Optics EXPRESS

31. X. Yin, L. Dong, H. Zheng, X. Liu, H. Wu, Y. Yang, W. Ma, L. Zhang, W. Yin, L. Xiao, and S. Jia, "Impact of Humidity on Quartz-Enhanced Photoacoustic Spectroscopy Based CO Detection Using a Near-IR Telecommunication Diode Laser," Sensors **16**(2), 162 (2016).
32. P. Patimisco, A. Sampaolo, M. Giglio, S. Dello Russo, V. Mackowiak, H. Rossmadl, A. Cable, F. K. Tittel, and V. Spagnolo, "Tuning forks with optimized geometries for quartz-enhanced photoacoustic spectroscopy," Opt. Express **27**(2), 1401–1415 (2019).
33. S. Li, L. Dong, H. Wu, A. Sampaolo, P. Patimisco, V. Spagnolo, and F. K. Tittel, "Ppb-Level Quartz-Enhanced Photoacoustic Detection of Carbon Monoxide Exploiting a Surface Grooved Tuning Fork," Anal. Chem. **91**(9), 5834–5840 (2019).
34. M. Giglio, A. Elefante, P. Patimisco, A. Sampaolo, F. Sgobba, H. Rossmadl, V. Mackowiak, H. Wu, F. K. Tittel, L. Dong, and V. Spagnolo, "Quartz-enhanced photoacoustic sensor for ethylene detection implementing optimized custom tuning fork-based spectrophone," Opt. Express **27**(4), 4271–4280 (2019).
35. S. Lee, J.-Y. Lee, and T.-S. Park, "Fabrication of SMD 32.768 kHz tuning fork-type crystals: Photolithography and selective etching of an array of quartz tuning fork resonators," Mater. Corros. **52**(9), 712–715 (2001).
36. P. Patimisco, G. Scamarcio, F. K. Tittel, and V. Spagnolo, "Quartz-Enhanced Photoacoustic Spectroscopy: A Review," Sensors **14**(4), 6165–6206 (2014).
37. K. Liu, X. Guo, H. Yi, W. Chen, W. Zhang, and X. Gao, "Off-beam quartz-enhanced photoacoustic spectroscopy," Opt. Lett. **34**(10), 1594–1596 (2009).
38. P. Patimisco, A. Sampaolo, L. Dong, M. Giglio, G. Scamarcio, F. K. Tittel, and V. Spagnolo, "Analysis of the electro-elastic properties of custom quartz tuning forks for optoacoustic gas sensing," Sens. Actuators, B **227**, 539–546 (2016).
39. L. Dong, A. A. Kosterev, D. Thomazy, and F. K. Tittel, "QEPAS spectrophones: design, optimization, and performance," Appl. Phys. B: Lasers Opt. **100**(3), 627–635 (2010).
40. T. L. Cottrell and J.C. McCoubrey, *Molecular Energy Transfer in Gases* (Butterworths, 1961).